Journal of Solid State Chemistry 183 (2010) 1853–1862

Contents lists available at ScienceDirect

Journal of Solid State Chemistry

journal homepage: www.elsevier.com/locate/jssc

Defect structure, electronic conductivity and expansion of properties of $(La_{1-x}Sr_x)_sCo_{1-y}Ni_yO_{3-\delta}$ ☆

Per Hjalmarsson *, Martin Søgaard, Mogens Mogensen

Fuel Cells and Solid State Chemistry Department, Risø National Laboratory for Sustainable Energy, Technical University of Denmark, Fredrikborgsvej 399, DK-4000 Roskilde, Denmark

ARTICLE INFO

Article history:
Received 27 April 2009
Received in revised form
12 March 2010
Accepted 30 April 2010
Available online 8 June 2010

Keywords:
Electronic conductivity
Lattice expansion
Mobility
Itinerant electron model
Lanthanum strontium cobaltite
Lanthanum strontium cobalt nickel oxide

ABSTRACT

This study reports on oxygen nonstoichiometry, electronic conductivity and lattice expansion of three compositions as function of T and P_{O_2} in the $(La_{1-x}Sr_x)_sCo_{1-y}Ni_yO_{3-\delta}$ ($x=0.1$, $y=0.4$; $x=0.1$, $y=0.3$; $x=0.2$, $y=0.2$) materials system. The nonstoichiometry data were successfully fitted using the *itinerant electron model* which indicates the existence of delocalized electronic states. This was also reflected in the high electronic conductivities, above 1000 S cm^{-1}, measured for all three compositions. The electronic conductivity was shown to decrease linearly with the oxygen nonstoichiometry parameter, δ, supporting that the conductivity is dependent on p-type charge carriers. Comparing calculated p-type mobilities with data reported in literature on $La_{1-x}Sr_xCoO_3$ indicated that Ni-substitution into $(La_{1-x}Sr_x)_sCoO_{3-\delta}$ increases the p-type mobility. The electronic conductivity was also found to be dependent on *intrinsic* charge related to spin excitations and Ni substitution rather than the *p*-type charge. A conductivity mechanism is hypothesized including a metallic like conductivity of the p-type charge and a small polaron conductivity of the *intrinsic* charge. Lattice expansion as function of T and δ was successfully described using first and second order thermal and chemical expansion coefficients. Substituting 10% Co with Ni in $(La_{0.6}Sr_{0.4})_{0.99}CoO_{3-\delta}$ was found to decrease the apparent thermal expansion with about 25%.

1. Introduction

Sr substituted $LaCoO_3$ has attracted broad attention due to interesting properties, such as electronic spin transitions, metallic like conductivity and its the ability to host vacancies in the oxygen sublattice [1–12]. The Sr^{2+} oxidizes the Co^{3+} ion partially which in turn introduces delocalized electronic states. The electronic structure in $(La_{1-x}Sr_x)_sCoO_{3-\delta}$ is also dependent on electronic spin on the Co^3, which influences both magnetic, conductive and expansion properties. Additionally, partial substitution of Co with Ni on *B*-site introduces further change in the electronic structure of the perovskite [13,14].

The degree of the Co oxidation is not fixed but a function of T and P_{O_2} and is related to oxygen vacancy formation via the electro neutrality principle. Also the degree spin transition on the Co^{3+} ion is a function of T and P_{O_2} and this allows us to study the electronic and defect structure in more detail. The electronic structure and the oxygen vacancies have been correlated in various defect models [8,10,15]. The *itinerant electron model* developed by Lankhorst and coworkers is the one receiving the broadest acceptance and appears to describe the defect chemistry of $(La_{1-x}Sr_x)_sCoO_{3-\delta}$ and related compounds well [16].

A number of papers have measured and analyzed the electronic conductivity (σ) of these materials with respect to T, P_{O_2}, δ and lattice parameters in an attempt to describe the conduction mechanisms but no clear consensus has emerged so far. Literature indicate instead that several materials properties might affect the electronic conductivity of $(La_{1-x}Sr_x)_sCoO_{3-\delta}$ as σ has been correlated with both Sr substitution levels, oxygen nonstoichiometry and bond angles [1,6,17].

Expansion of the lattice is not only dependent on the temperature dependency of its atomic vibrations but also on its the electronic and defect structure. Reduction of the Co^{4+} to Co^{3+} at increasing temperatures or decreasing P_{O_2} expands its Shannon radii and thus also the lattice. Additionally, the spin transitions have been argued to add an extra dimension to the lattice expansion as transitions from electronic low spin to intermediate or high spin states increase the Shannon radii of the Co ions [18]. The strain of $(La_{1-x}Sr_x)_sCoO_{3-\delta}$ as function of T, P_{O_2} and x has been reported in several studies in which the total *apparent* thermal expansion is often separated into a thermal and chemical expansion contribution [6,19–22]. The chemical

☆This work is supported by the Danish Research Agency, the program committee for Nanoscience and Technology, Biotechnology and Information Technology (NABIIT), Grant no. 2106-05-0033.

* Corresponding author. Fax: +45 4677 5858.
E-mail address: phja@risoe.dtu.dk (P. Hjalmarsson).

0022-4596/$ - see front matter © 2010 Elsevier Inc. All rights reserved.
doi:10.1016/j.jssc.2010.04.044

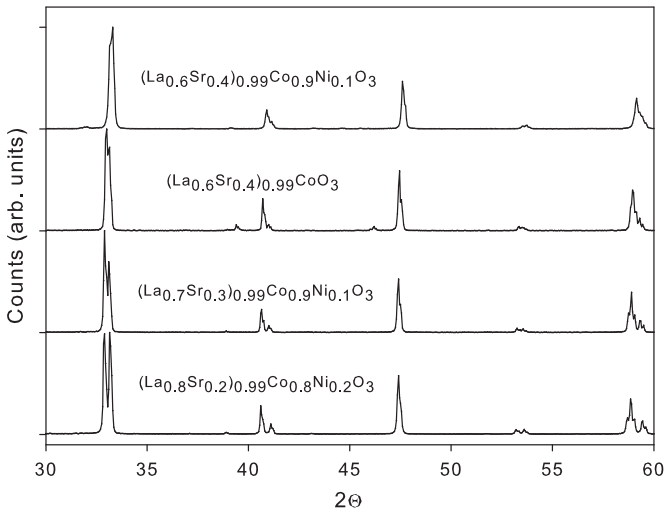

Fig. 1. Powder X-ray diffraction pattern of the studied compositions.

expansion coefficient is related to the oxygen nonstoichiometry, which in turn is associated with the Co^{4+}/Co^{3+} ratio through the electro neutrality principle [23].

Partial substitution of Co with Ni in $(La_{1-x}Sr_x)_sCoO_{3-\delta}$ has earlier been shown to increase electronic conductivity [24,25] and decrease lattice expansion [26], properties which are of technological interest for instance in solid oxide fuel cells (SOFCs). We have studied the electronic and expansion properties of the compositions $(La_{0.8}Sr_{0.2})_{0.99}Co_{0.8}Ni_{0.2}O_{3-\delta}$, $(La_{0.7}Sr_{0.3})_{0.99}Co_{0.9}Ni_{0.1}O_{3-\delta}$ and $(La_{0.6}Sr_{0.4})_{0.99}Co_{0.9}Ni_{0.1}O_{3-\delta}$ in more detail in an attempt to clarify the effect of Ni substitution in $(La_{1-x}Sr_x)_sCoO_{3-\delta}$. We have also studied the concentration oxygen vacancies (δ) in these compositions as function of T and P_{O_2} in order to test whether their defect structure can be described by the *itinerant electron model* [16]. The results are discussed with respect to results in recent literature.

2. Experimental

Powder and dense sintered bars of $(La_{0.6}Sr_{0.4})_{0.99}CoO_{3-\delta}$ (LSC40), $(La_{0.7}Sr_{0.3})_{0.99}Co_{0.9}Ni_{0.1}O_{3-\delta}$ (LSCN3010), $(La_{0.6}Sr_{0.4})_{0.99}Co_{0.9}Ni_{0.1}O_{3-\delta}$ (LSCN4010) and $(La_{0.8}Sr_{0.2})_{0.99}Co_{0.8}Ni_{0.2}O_{3-\delta}$ (LSCN2020) were fabricated as described in [27]. The abbreviated notations in brackets will be used throughout the paper. An exact stoichiometric A/B ratio of one is practically impossible to synthesize as it is impossible to weigh the starting compounds in such an exact manner. We have for this reason deliberately chosen an A/B-ratio of 0.99 in order to know which type of secondary phases to expect. The stoichiometric accuracy is such that we can assume the composition to be A-site substoichiometric. Bars used for electronic conductivity measurements were cut to dimensions of approximately $2 \times 2 \times 25\,mm^3$ whereas bars used in the dilatometry measurements were of the dimensions $4 \times 4 \times 20\,mm^3$. Geometrically measured densities of the sintered samples were above 95% of theoretical density calculated from XRD data. A STOE Theta-Theta diffractometer (40kV, 30 mA) was used for X-ray diffraction measurements (Fig. 1). Powder samples were analyzed thermogravimetrically with a NETZSCH STA 409C/CD in order to estimate oxygen nonstoichiometry as a function of temperature. 300 mg of powder sample was heated and cooled in $50\,ml\,min^{-1}$ airflow to 1300 °C with a heating rate of $10\,°C\,min^{-1}$. Cooling rate was set to $1\,°C\,min^{-1}$ down to 600 °C followed by a rapid cooling of $10\,°C\,min^{-1}$ to room temperature. Data was taken from the cooling ramp of the measurement (oxidation). A differential NETZSCH TG 439 was used to measure oxygen nonstoichiometry as function of P_{O_2} at 4–5 different temperatures in the range 600–1000 °C. About 40 mg of powder was used in the experiments. Powder samples equilibrated within less than one minute as seen in Fig. 2. The weight of the sample was measured for 2 h after each change in P_{O_2} to assure that the stoichiometric change was fully equilibrated. In some cases long term transients were observed. Data from these transients (T, P_{O_2}) were not used in the fitting of measured stoichiometry changes to theoretical defect chemistry models. Data from oxidative (increasing) steps in P_{O_2} were used in the defect chemistry analysis.

Expansion measurements were carried out on sintered bars with a NETZSCH DIL 402C. The temperature was scanned from room temperature to 1300 °C with $2\,ml\,min^{-1}$ and in airflow of $50\,ml\,min^{-1}$. Data were taken from the cooling ramp of the measurement (oxidation). Expansion measurements as function of P_{O_2} were carried out at 700–1000 °C from $P_{O_2} \approx 0.21 - 0.005$ atm. The samples relaxed for 2–4 h after each step change in P_{O_2} to assure that equilibrium had been reached. Equilibrated expansion data were taken from the oxidative (increasing) P_{O_2} −steps. Fig. 3 shows the results of a typical expansion measurement.

The electrical conductivity was measured with a four point probe DC-technique. Sintered bars were wired with platinum

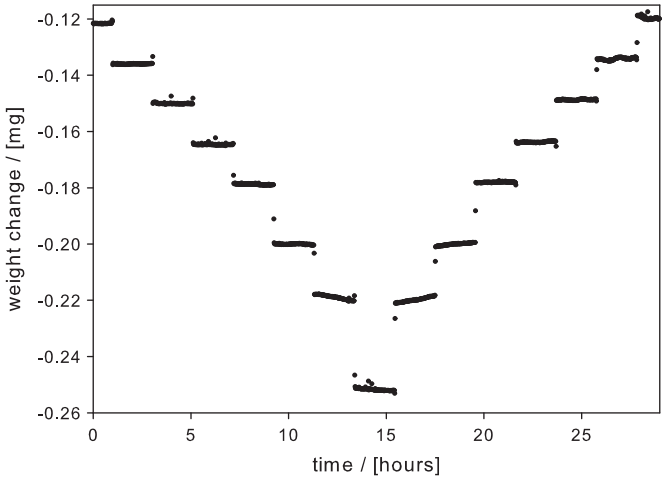

Fig. 2. Weight equilibration upon sudden changes in oxygen partial pressure at 750 °C for LSCN4010. $\Delta(\log P_{O_2})$ is approximately 0.15.

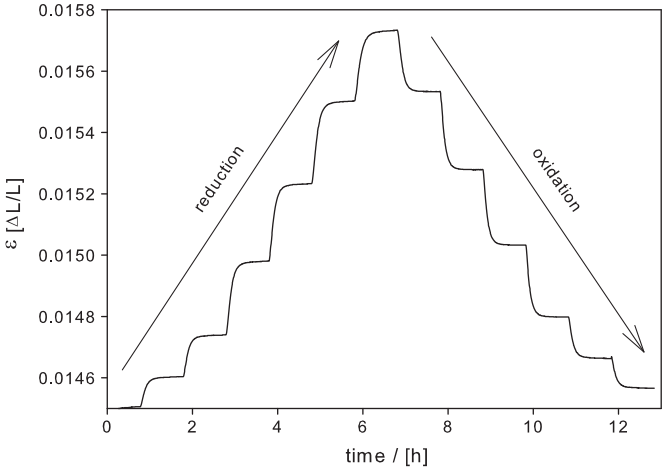

Fig. 3. Expansion equilibrations upon changes in P_{O_2} at 800 °C for LSCN4010; $\Delta(\log P_{O_2})$.

threads and painted with platinum paste at both ends. The resistance was measured with a Keithley 2700 multimeter. Voltage probes were separated 0.5 cm apart and measurements were performed at temperatures ranging from 700 to 1000 °C and P_{O_2} from 0.21–0.001 atm. In all experiments the P_{O_2} was controlled by mixing of N_2 and O_2.

Equilibrium was considered reached in all experiments if the relative change was less than about one percentage within 30 min. The measurement under this specific condition has not been reported in this paper if equilibrium was not reached.

3. Results

3.1. Electronic and defect structure

Thermogravimetric (TG) analysis as function of both temperature and P_{O_2} was conducted on powder samples in order to study the oxygen nonstoichiometry parameter, δ. This parameter corresponds the fraction of missing oxide ions per perovskite formula unit. Fig. 4 plots changes in δ for LSC40, LSCN4010, LSCN3010 and LSCN2020 as function of temperature. The onset temperature of lattice oxygen loss is seen to increased with decreasing Sr content. This has been discussed in more detail for $(La_{1-x}Sr_x)_sCo_{1-y}Ni_yO_{3-\delta}$ in a previous study to which the reader is referred for further details [27]. Comparing LSC40 and LSCN4010 allows us to study the effect of Ni substitution on *B*-site in LSC40. Both compositions were shown to have approximately the same the onset temperature of oxygen loss. However, a different behavior is observed above the onset temperature where δ increases more strongly with T for LSCN4010 as compared to LSC40. Above 800 °C the increase in δ is approximately linear with respect to temperature with coefficients of $4.3\times10^{-4}K^{-1}$ for LSCN4010 and $3.1\times10^{-4}K^{-1}$ for LSC40. Included in Fig. 4 is also the predicted δ calculated using the *itinerant electron model* as describe further below. The results show good agreement between calculated oxygen nonstoichiometry and measured data for LSCN2020 and reasonable agreements for LSCN4010 and LSCN3010.

The *itinerant electron model* [10] is today the most widely used defect model for mixed ionic and electronic conductors (MIECs) such as $(La_{1-x}Sr_x)_sCoO_{3-\delta}$. This particular materials shows high electronic, "metallic-like" conductivity, which is indicative of substantial levels of delocalized electronic charge. In this model electrons from the oxidation of oxide ions are transferred into a conduction band which raises the Fermi level. This means that the positive charge introduced by Sr substitution in $(La_{1-x}Sr_x)_sCo_{1-y}Ni_yO_{3-\delta}$ is not associated with the Co ion but is free to move as a delocalized charge carrier. It means further that the entropy of the electrons and defect–defect interactions can be neglected. The relationship between the oxygen nonstoichiometry in an oxide and the chemical potential of oxygen is expressed in

$$\mu_{O_2}=\Delta E_{ox}-\frac{4(2[V_O^{\bullet\bullet}]-[Sr_{La}'])}{g(E_F)}-T\Delta S_{ox}-2RT\ln\left(\frac{[V_O^{\bullet\bullet}]}{(3-[V_O^{\bullet\bullet}])}\right) \quad (1)$$

ΔE_{ox} and ΔS_{ox} are the energy and entropy associated with filling two vacancies with an oxygen molecule from vacuum and simultaneously adding four electrons at the fermi level. $g(E_F)$ is the density of states at the Fermi level, which is the number of states available for occupation at this specific energy level. $[V_O^{\bullet\bullet}]$ is the concentration of oxygen vacancies and related to the oxygen nonstoichiometry parameter as $\delta=3[V_O^{\bullet\bullet}]$. μ_{O_2} is a function of T and P_{O_2} calculated using the empirical expression according to [28]

$$\mu_{O_2}^{gas}=\mu_{O_2}^{0,gas}+RT\ln(P_{O_2}) \quad (2)$$

$$\mu_{O_2}^{0,gas}=RT\left(n_1+\frac{n_2}{T}+n_3\ln(T)+n_4\ln(1-e^{-n_5/T})\right) \quad (3)$$

where T and P_{O_2} are found in K and in atm $n_1=-1.225$, $n_2=-1045$ K, $n_3=-3.5$, $n_4=1.013$, $n_5=2242$ K [28].

The change in oxygen nonstoichiometry was measured isothermally as function of P_{O_2} at various temperatures between 600 and 1000 °C for the compositions LSCN2020, LSCN3010 and LSCN4010. These data are reported in Figs. 5–7, where the solid lines represent the best linear least square fit to the *itinerant electron model*. Our experimental data shows reasonably good agreement to the model. The parameters ΔE_{ox}, ΔS_{ox} and $g(\varepsilon_F)$ are reported in Table 1 together with data for LSC40 reported in [6] and $La_{0.8}Sr_{0.2}CoO_{3-\delta}$ [10]. Table 1 also shows the sum of square deviations, χ_δ which is defined as $(\Sigma(\log P_{O_2,measured(i)}-\log_{O_2,calculated(i)})^2)/(N-3)$, where N is the total number of measurements ($N=32$–50) and $P_{O_2,measured(i)}$ is the measured P_{O_2} of the *i*'th measurement.

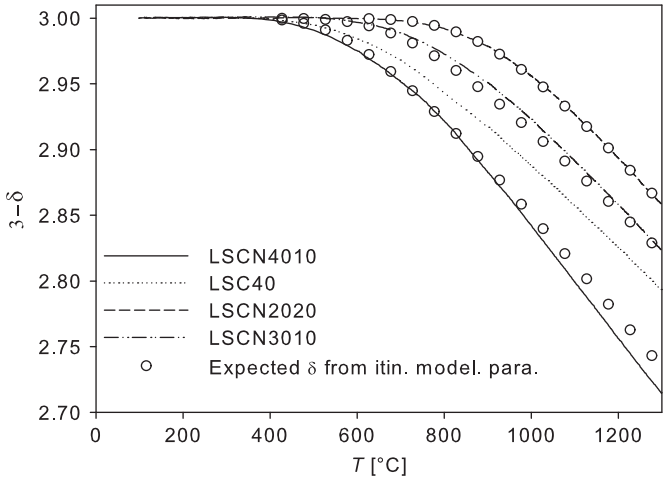

Fig. 4. $3-\delta$ as function of temperature for LSCN4010, LSC40, LSCN3010 and LSCN2020. Rings denote predicted oxygen nonstoichiometry calculated for the three Ni containing samples using the *itinerant electron model*. Substituting 10% Co with Ni in LSC40 increases the linear trend with which oxygen vacancies are formed upon heating whereas increasing [Sr] in LSCN3010 to 40% lowers the onset temperature of lattice oxygen loss.

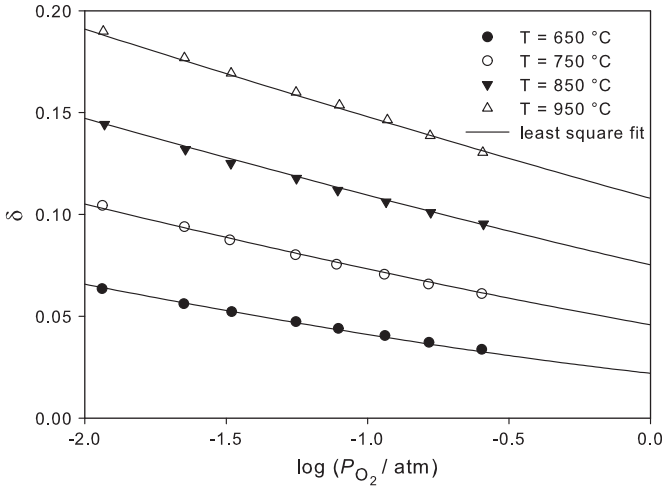

Fig. 5. δ as function of P_{O_2} for LSCN4010 at various temperatures. Lines represent best fit to the *itinerant electron model* (see Eq. (1)).

3.2. Electronic conductivity

The electrical conductivity of LSCN2020, LSCN3010 and LSCN4010 was measured as function of temperature and P_{O_2}. In the temperature range (100–1000 °C) and P_{O_2} range (0.001–1 atm) the electrical conductivity was 1000–2000 S cm^{-1} for all compositions. The ionic conductivity of these materials is lower than 1 S cm^{-1} [29], and consequently the transference number is approximately unity. Thus the measured electrical conductivity can be approximated as the electronic conductivity of the materials. Substituting SrO into $LaCoO_3$ is effectively a p-type doping as positive holes are introduced when Co is oxidized. This explains the substantial increase in the measured electronic conductivity with increasing x in $(La_{1-x}Sr_x)_sCoO_{3-\delta}$ [1].

The oxygen nonstoichiometry was calculated using the *itinerant electron model* and the fitting parameters listed in Table 1 for each composition and at each condition (T, P_{O_2}) the conductivity was measured. The conductivity as function of δ is plotted in Figs. 8–10 for the three compositions, LSCN2020, LSCN3010 and LSCN4010. At increasing T or decreasing P_{O_2} Co undergoes reduction, which increases δ at the expense of p-type charge carriers, c_p. This occurs as a consequence of the

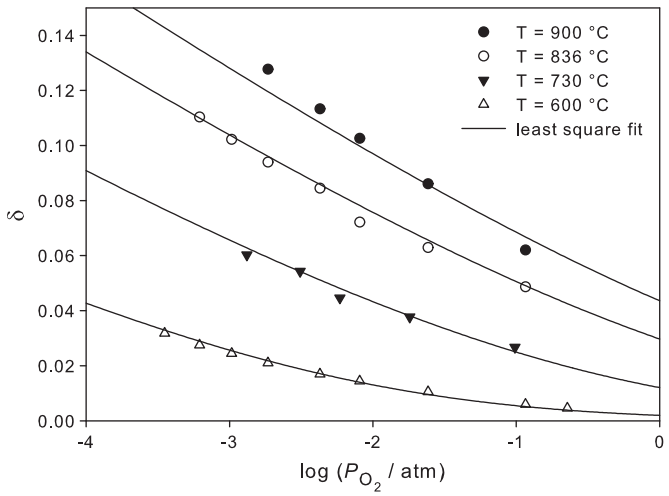

Fig. 6. δ as function of P_{O_2} for LSCN3010 at various temperatures. Lines represent best fit to the *itinerant electron model* (see Eq. (1)).

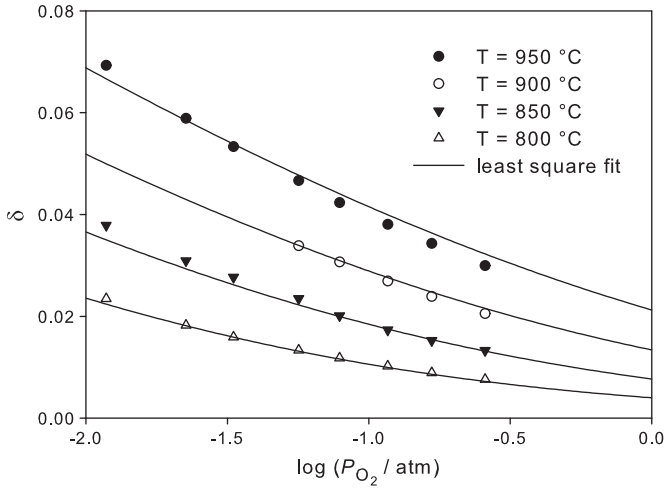

Fig. 7. δ as function of P_{O_2} for LSCN2020 at various temperatures. Lines represent best fit to the *itinerant electron model*. (see Eq. (1)).

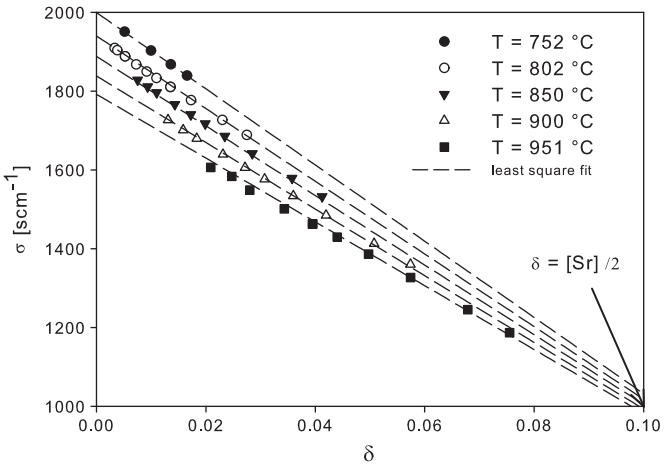

Fig. 8. Electronic conductivity as function of δ for LSCN2020. Lines represent best fit to Eq. (5).

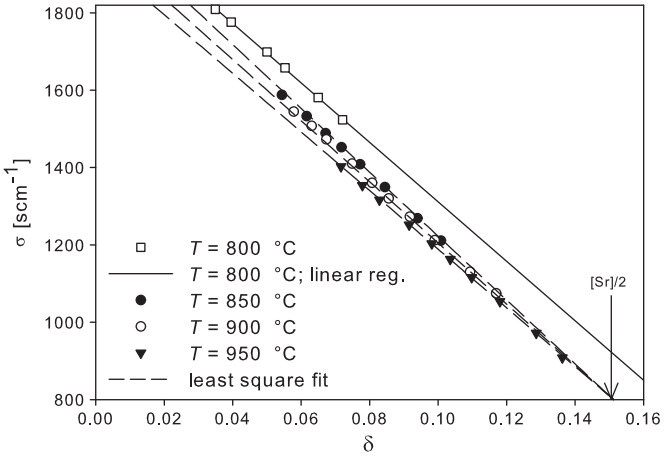

Fig. 9. Electronic conductivity as function of δ for LSCN3010. Lines represent best fit to Eq. (5). The lowest temperature could not be fitted to the conductivity model and have instead been regressed linearly to calculated the p-type mobility.

Table 1
Least square fitting parameters to the *itinerant electron model* for LSCN2020, LSCN3010, LSCN4010 and LSC40 [6,10].

	ΔE_{ox} (kJ mol^{-1})	Δ_{ox} (J mol^{-1} K^{-1})	$g(\varepsilon_F)$ (kJ^{-1} mol)	χ_δ
LSCN2020	−320.5	76.4	0.0168	0.0037
LSCN3010	−299.0	88.9	0.0148	0.0149
LSCN4010	−261.3	98.1	0.0192	0.0011
LSC40 [6]	−217.2	141.2	0.0188	
$La_{0.8}Sr_{0.2}CoO_{3-\delta}$ [10]	−334.1	69.5	0.0159	

ΔE_{ox} and ΔS_{ox} are the enthalpy and entropy of molecular oxygen in the oxide. $g(\varepsilon_F)$ is the density of states at the Fermi level.

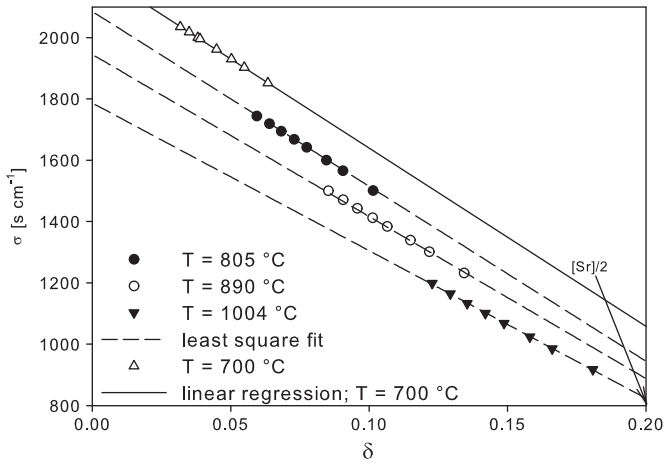

Fig. 10. Electronic conductivity as function of δ LSCN4010. Lines represent best fit to Eq. (5). The lowest temperatures could not be fitted to the conductivity model and have instead been regressed linearly to calculated the p-type mobility.

electro-neutrality principle expressed in Reaction (4). Consequently, c_p is expected to be a function of T and P_{O_2} and should in theory equal zero at the conditions where $2\delta = [Sr'_{La}]$. Figs. 8–10 shows clearly that σ decreases linearly with δ which strongly supports a p-type conductivity in these compositions.

However, the results also show a substantial conductivity at the conditions where c_p is zero, which indicate that the p-type conductivity cannot fully describe the conductive behavior alone. Nominal $LaCoO_3$ is known to conduct charge at high temperatures due to transitions from low to intermediate or high spin state on the Co ions which excites electrons to a narrow itinerant band [30]. $LaNiO_3$ is a reasonable electronic conductor already at room temperature due to one delocalized electron in the *d*-orbitals of the Ni-ions (the electronic structure, $t_{2g}^6 e_g^1$, is discussed in [31,27] to which the reader is referred for further details). It is therefore a fair assumption that there is also an *intrinsic* contribution to the total electronic conductivity, which is independent on p-type charge carriers introduced by Sr substitution. This has led us to discriminate between two different contributions to the total conductivity.

(1) The p-type *conductivity* which is related to the Sr content and the concentration of oxygen vacancies.
(2) The *intrinsic* conductivity which is *not* dependent on the degree of Co reduction and Sr content. This conductivity is believe to arise mainly from spin transitions on the Co ions and from the extra electron introduced by the Ni substitution:

$$2Co_{Co}^{\cdot} + O_O^X \rightarrow \tfrac{1}{2}O_2(g) + V_O^{\bullet\bullet} + 2Co_{Co}^X \quad (4)$$

In an attempt to describe our measured electronic conductivities using these two types of conductivity we hypothesized on a simple conductivity mechanism. The mobility of charge carriers in a metal is known to decrease with increasing temperature [32]. $(La_{1-x}Sr_x)_sCoO_{3-\delta}$ is known to have a metallic-like temperature dependence [6] and Ni substitution is known to increase the metallic character further [24], thus all our compositions can be considered metallic-like. As a starting point we have therefore used an approximate "mechanism" expressed in Eq. (5), which assumes that both the p-type and the *intrinsic* conductivity has a "metallic like", reciprocal temperature dependence:

$$\sigma = C([Sr'_{La}] - 2\delta)\frac{\mu_{ext}}{T} + \left(\frac{\sigma_{int.}}{T} + \sigma_{const.}\right)_{2\delta = [Sr'_{La}]} \quad (5)$$

$C([Sr'_{La}] - 2\delta)$ is the concentration of charge carriers (c_p). $C = \rho N_A e/M$, where M is the molar mass of the perovskite, ρ is the density, N_A is the Avogadro number and e is the elementary charge. μ_{c_p} is the mobility of the p-type charge carriers, σ_1 and σ_2 are the temperature dependent and temperature independent contributions to the intrinsic conductivity.

Table 2
Least square fitting parameters to the Eq. (5) for LSCN2020, LSCN3010, LSCN4010.

	C (C cm^{-3})	μ_{c_p} (cm^2 V^{-1} s^{-1} K)	σ_1 (S cm^{-1} K^{-1})	σ_2 (S cm^{-1})	χ_σ
LSCN2020	2860	1734	3.15×10^5	724	24
LSCN3010	2844	1630	–	809	22
LSCN4010	2850	1079	8.37×10^5	168	26
LSC40 [6]	2835	1023	–	–	–

The extrinsic mobility of LSC40 is included from Refs. [6] for comparison. C is coulomb.

The dashed lines in Figs. 9 and 10 represent the best linear least square fit to Eq. (5). The solid lines are linear regressions of the conductivity of the lowest temperature as these data could not be satisfactorily included in the model. The conductivity data for LSCN3010 at 800 °C and LSCN4010 at 700 °C still showed very linear correlation with δ but measured higher p-type mobilities (approximately 2900 and 2000 cm^2 V^{-1} s^{-1} for LSCN3010 and LSCN4010, respectively). Measured conductivities at all other temperatures could be fitted with good accuracy to Eq. (5) and the resulting parameters listed in Table 2. Table 2 also shows the sum of square deviations, χ_σ which is defined as $(\Sigma(\sigma_{measured,(i)} - \sigma_{calculated,(i)})^2)/(N-3)$, where N is the total number of measurements (N=43) and $\sigma_{measured,(i)}$ is the conductivity of the i'th measurement.

As seen in Fig. 9 the fitted conductivities of LSCN3010 intercepts almost exactly at $\delta = [Sr]/2$ implicating that the intrinsic conductivity of this composition is independent on temperature within this T-range. It should be stressed that the data points are lying relatively close to each other and that the conductivity model includes as many as three fitting parameters. Especially σ_1 and σ_2 are associated with great uncertainty as they are fitted based on only 3 (LSCN3010 and LSCN4010) and 5 (LSCN2020) data points all lying within a narrow temperature range.

3.3. Thermal and chemical expansion

Fig. 11 plots the apparent thermal expansion coefficient (TEC), calculated by differentiating the strain, ε, with respect to temperature. The expansion measurement for LSC40 was reported in an earlier paper [27] in which the sharp drop in TEC at around 800 °C was attributed to the reduction $Co_3O_4 \rightarrow CoO$ of the inevitable traces of secondary Co oxide phases. Two sharp peaks were found in the expansion measurement of LSCN4010. These peaks were not observed in any of the Ni containing compositions in the previous paper nor in the repetitive measurement to only 1100 °C instead of 1300 °C.

Adler et al. [21] have developed a expansion model for nonstoichiometric mixed conducting perovskites such as $(La_{1-x}Sr_x)_sCoO_{3-\delta}$, which takes into account first and second order expansion with respect to both the temperature and oxygen stoichiometry. The expansion model is expressed in Eq. (6).

$$\varepsilon(T,\delta) - \varepsilon(T_0, \delta = 0) = (\alpha_1 + \alpha_2(T - T_0))(T - T_0) + (\beta_1 + \beta_2\delta)\Delta\delta \quad (6)$$

where $\varepsilon = \Delta L/L_0$ is the uniaxial strain, α_1 and α_2 are the first and second order thermal expansion coefficients and β_1 and β_2 are the first and second order chemical expansion coefficients [21].

The lattice expansion of LSCN3010, LSCN4010 and LSC40 was measured as function of P_{O_2} at 700, 800, 900 and 1000 °C. The oxygen nonstoichiometry was calculated using the *itinerant*

electron model and the fitting parameters listed in Table 1 for at each condition (T, P_{O_2}) at which the expansion was measured. The lattice expansion has been plotted as function of δ in Figs. 12–14.

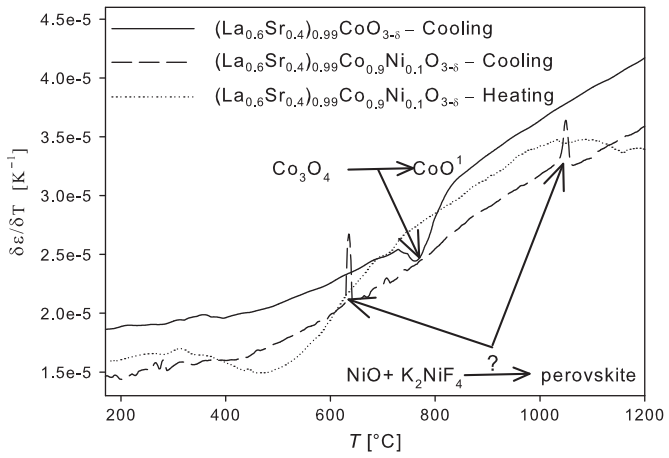

Fig. 11. The apparent TEC as function of temperature for LSCN4010 and LSC40. Substituting 10% Co with Ni in LSC40 appears to decrease the TEC substantially. Peaks in the TEC of LSCN4010 are possibly associated with phase transitions of secondary phases.

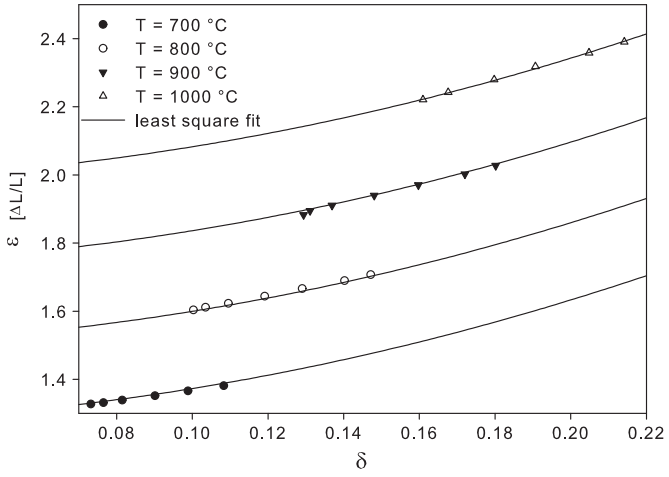

Fig. 12. Strain as function of δ and T for LSC40. Lines represent best fit to Eq. (6).

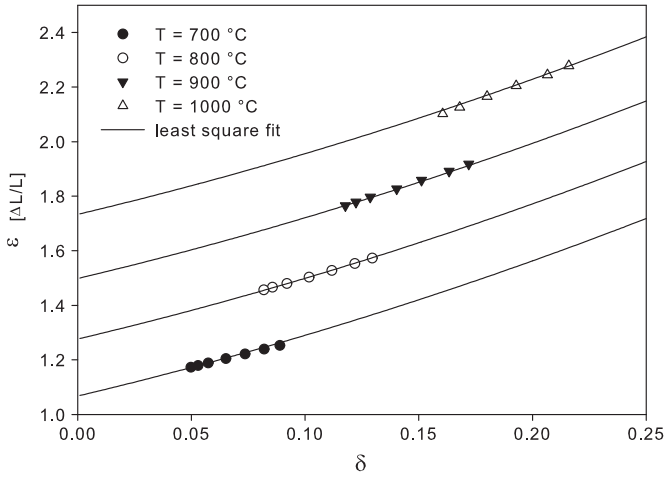

Fig. 13. Strain as function of δ and T for LSCN4010. Lines represent best fit to Eq. (6).

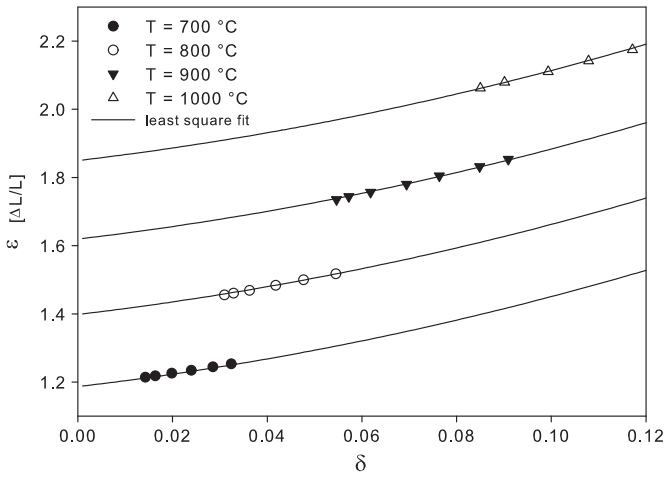

Fig. 14. Strain as function of δ and T for LSCN3010. Lines represent best fit to Eq. (6).

Table 3
First and second order thermal and chemical expansion coefficients extracted as the best least square fitting parameters to the expansion model expressed in Eq. (6) [21].

	$\alpha_1+\alpha_2(T-T_0)$ (K^{-1})	$\beta_1+\beta_2\delta$	χ_ε
LSCN3010	$14.4\times10^{-6}+4.65\times10^{-9}(T-T_0)$	$0.0163+0.101\delta$	5.0×10^{-6}
LSCN4010	$11.4\times10^{-6}+6.54\times10^{-9}(T-T_0)$	$0.0197+0.0251\delta$	3.0×10^{-6}
LSC40	$15.5\times10^{-6}+4.93\times10^{-9}(T-T_0)$	$0.0193+0.0803\delta$	2.3×10^{-6}
LSC40 [21]	$14.20\times10^{-6}+4.84\times10^{-9}(T-T_0)$	$0.0183+0.270\delta$	

The model was applied to our expansion data and the best linear least square fits to Eq. (6) is shown as the solid lines. The least square fitting parameters are listed as the first and second order thermal and chemical expansion coefficients in Table 3. Table 3 also shows the sum of square deviations, χ_ε which is defined as $(\Sigma(\varepsilon_{measured,(i)}-\varepsilon_{calculated,(i)})^2)/(N-3)$, where N is the total number of measurements ($N=25$–28) and $\varepsilon_{measured,(i)}$ is the expansion of the i'th measurement.

The lower TEC of LSCN4010 as compared to LSC40 seen in Fig. 11 is also reflected in the expansion coefficients listed in Table 3.

4. Discussion

4.1. Electronic and defect structure

It is evident from Fig. 4 that substitution of La with Sr increases the concentration of vacancies in the oxygen sublattice above an onset temperature of approximately 500 °C. The oxygen non-stoichiometry parameter of LSCN4010 is more than twice as large as that of LSCN3010 between 500 and 800 °C. This can be understood as LSCN4010 having a higher degree Co in its reduced form, Co^{4+}, at room temperature which can undergo thermal reduction upon heating and consequently form oxygen vacancies. This effect is well known and will therefore not be discussed in detail here [2,27] but it is interesting to note that this trend also holds when Ni is present on the *B*-site of the perovskite.

Increasing the Ni content appears also to increase the oxygen nonstoichiometry at high T as substituting 10% Co with Ni in LSC40 increases the linear tendency with which oxygen vacancies are created upon heating. This stand in sharp contrast to results of Teraoka et al., who have found that substituting 20% Co with Ni in $(La_{0.6}Sr_{0.4})CoO_{3-\delta}$ decreases the oxygen nonstoichiometry

parameter [33]. It is not relevant to ascribe a valency to the Co ion in this configuration as the charge on Co ions are delocalized. Instead it is probably more correct to refer to an average oxidation state, which will be somewhat higher in LSCN4010 than in LSC40 at room temperature. This fact could possibly results in a higher tendency to undergo thermal reduction, in analogy with the above discussed comparison between LSCN3010 and LSCN4010.

The relatively good agreements of the measured nonstoichiometry in LSCN2020, LSCN3010 and LSCN4010 to the *itinerant electron model* indicates that these compositions incorporates delocalizes electronic charge. This is also in agreement with the high electronic conductivities measured for these compositions. However, its difficult to make further interpretations of the parameters $g(\varepsilon_F)$, ΔE_{ox} and ΔS_{ox}.

The *itinerant electron model* does not take into account charge disproportionation of the kind $2Co_{Co}^{x} \rightarrow Co_{Co}^{\cdot} + Co_{Co}^{\prime}$ and thus assumes that the concentration of charge arising as a consequence of such as reaction is negligible compared to the p-type charge introduced by Sr substitution. The reasonably good fit of the stoichiometry data to the model indicate that this holds also in the case when Ni is present on *B*-site. We have in a previous study presented XANES measurements supporting that the reaction $Co^{iii} + Ni^{III} \rightarrow Co^{IV} + Ni^{2+}$ does not occur to any notable degree [27]. The XANES data in this study showed that Ni remained its valency state irrespective of the degree of Sr or Co in the crystal whereas Co was under strong influence of only [Sr] and not [Ni]. It was also shown support that it is exclusively Co that is reduced at increasing temperatures.

The clear linear correlation between σ and δ, calculated using the *itinerant electron model* indicates that the change in charge concentration as a result of P_{O_2} shifts is only associated with changes in the p-type charge described by the *itinerant electron model*. If charge disproportionation had occurred in $(La_{1-x}Sr_x)_sCo_{1-y}Ni_yO_{3-\delta}$ upon P_{O_2} shifts then the concentration of available charge and thus the conductivity would have been higher than predicted by the *itinerant electron model*.

4.2. Electronic conductivity

The conductivity as function of oxygen nonstoichiometry was shown to decrease linearly with increasing δ (see Figs. 8–10), which indicates that these compositions incorporates p-type charge carriers. It shows further that changes in its concentration as function of P_{O_2} has a much stronger impact on the conductivity as compared to any possible changes in the *intrinsic* charge carrier concentration. The *intrinsic* contribution to the conductivity is, however, substantial within the measured *T*-range, being approximately 800–1000 $S\,cm^{-1}$ for all three compositions. Fitting the conductivity data as function of both *T* and δ with the model expressed in Eq. (5) showed good agreement for LSCN2020. Also LSCN3010 and LSCN4010 were found to agree well with the conductivity model at all temperatures but the lowest. The results presented in Table 2 indicates that the mobility of the p-type charge carriers μ_{c_p} increases with decreasing Sr content. At 1000 °C the mobility of the p-type charge is about 1.1–1.6 $cm^2\,V^{-1}\,s^{-1}$ for LSCN4010 and LSCN3010, respectively. This trend is also in agreement with the p-type mobility reported for $(La_{1-x}\ Sr_x)_{0.99}CoO_{3-\delta}$ by Søgaard et al. [6]. For $(La_{0.85}Sr_{0.15})_{0.99}CoO_{3-\delta}$ the aforementioned study reports mobilities of 1.2–1.4 $cm^2\,V^{-1}\,s^{-1}$ in the range from 850 to 1000 °C. This can be compared with our calculated mobilities of 1.4–1.5 $cm^2\,V^{-1}\,s^{-1}$ for LSCN2020 in the same temperature range. Also the p-type mobility of LSCN4010 was found to be about 5% higher than that of LSC40. These comparisons indicate that Ni substitution in $(La_{1-x}Sr_x)_sCoO_{3-\delta}$ increases the mobility of the p-type charge carriers.

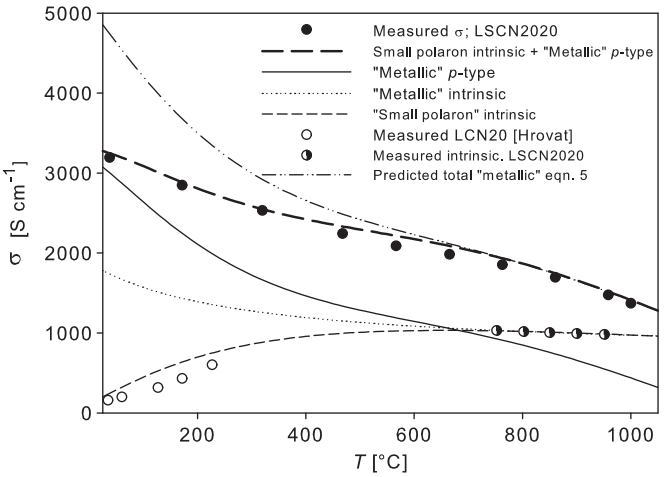

Fig. 15. Electric conductivity as function of temperature for LSCN2020. Lines represent best fit to Eq. (5), extrapolated down to room temperature with δ- values taken from Fig. 4. The fits shows reasonable agreement in temperature trend but deviates substantially in absolute values at low *T*.

Fig. 15 shows the *intrinsic* and p-type conductivity as well as the total conductivity from room temperature to 1000 °C, predicted using the results in Table 2 together with measured δ as function of temperature (see Fig. 4). Fig. 15 also shows the conductivity of the same composition as function of temperature but measured on a different sample with a different experimental setup. The predicted total conductivity, extrapolated on basis of the mechanism expressed in Eq. (5), was shown to correlate well with the measured data only above 700 °C. At lower temperatures it deviates substantially and overestimates the room temperature conductivity with almost 2000 $S\,cm^{-1}$ and hence the suggested equation does not seem to satisfactorily describe the conductivity mechanism. The temperature dependence of the p-type conductivity was determined based 43 data points. The delocalized p-type conductivity arises from the fact that the Co ions in LaCoO3 have been partially oxidized upon Sr substitution thus the presence of the p-type charge is not dependent on thermal excitations like for example charge associated with spin transitions. We therefore believe it is fair to assume that the p-type conductivity is of metallic character. A reciprocal temperature dependence has also been suggested previously for $(La_{1-x}Sr_x)_sCoO_{3-\delta}$ [6].

We postulate instead that the discrepancy between measured and predicted conductivity of LSCN2020 is related to the *intrinsic* conductivity mechanism. The predicted *intrinsic* conductivity, i.e. the conductivity at $[Sr] = \delta/2$, at 750–950 °C can be considered accurate within the precision of the experiments. However, the reliability when projected to lower *T* is more questionable. The *intrinsic* conductivity, as defined in this particular paper, is independent on the p-type charge carriers and any change in the *intrinsic* conductivity is instead assumed to be related to spin transitions on the Co ions. This is believed to have substantial effect on the conductivity and this correlation has been discussed in a previous paper for $(La_{1-x}Sr_x)_{0.99}Co_{0.6+x}Ni_{0.4-x}O_{3-\delta}$ [27,2]. It can be understood in the light of ligand field theory. When positioned in a octahedral geometry of a crystal, *d*-orbitals of a transition metal ion split into two *e*- and three *t*-orbitals, separated by a small band gap. The *e*-orbitals are oriented towards the *p*-orbitals of the oxygen ions to form overlap (bonds) that make up the conductive path ways. The overlap comes at the expense of a slightly higher energy than the *t*-orbitals, in the case

of $LaCoO_3$ of approximately 0.05 eV [34,30,35]. The thermodynamic consequence is that all six *d*-electrons of the Co^{3+} ion are preferably found in the three *t*-orbitals with no net electron spin. However, the band gap is sufficiently low for thermal energy to excite electrons. The electron will simultaneously change its spin following Hund's rule and transition from low spin Co(III), t_{2g}^6, to intermediate spin Co(iii) $t_{2g}^5e_g^1$ or high spin Co^{3+} $t_{2g}^4e_g^2$ occur at elevated temperatures. This increases the degree of the Co3d–O2p overlap that in turn allow charge transport through the crystal [36–42]. Octahedral Ni in $LaNiO_3$ has the low spin configuration, $t_{2g}^6e_g^1$ and thus one electron is already found in the conductive *e*-orbitals. This explains why $LaNiO_3$ shows metallic conductivity at room temperature while $LaCoO_3$ is only a reasonable conductor at much higher temperatures. This property, typical of $LaCoO_3$, gives also rise to interesting expansion properties discussed further below as well as in a previous study on $(La_{1-x}Sr_x)_sCo_{1-y}Ni_yO_{3-\delta}$:

$$\sigma = \frac{A}{T}\exp\left(\frac{-E_A}{kT}\right) \tag{7}$$

The electronic conductivity of $La_sCo_{1-x}Ni_xO_{3-\delta}$ with $x < 0.4$ has been argued by Huang et al. [24] to follow the small polaron conduction as expressed in Eq. (7). Fitting the *intrinsic* conductivity data of LSCN2020 to this equation yields an activation energy of 0.07 eV. Huang et al. have determined the small polaron activation energy to range from 0.05 to 0.07 eV for related compositions [24]. An *intrinsic* conductivity predicted on basis of the small polaron conductivity has been included in Fig. 15 as well as the conductivity of $LaCo_{0.8}Ni_{0.2}O_3$ measured from room temperature to 175 °C by Hrovat et al. [25]. This composition corresponds, in theory, to the LSCN2020 but without p-type charge as there is no Sr^{2+} that have oxidized the Co ions. Hence the *intrinsic* conductivity of LSCN2020 should roughly correspond to that of $LaCo_{0.8}Ni_{0.2}O_3$. As seen in Fig. 15 the predicted *intrinsic* small polaronic conductivity of LSCN2020 agrees reasonably well with that of $LaCo_{0.8}Ni_{0.2}O_3$. Adding the predicted *intrinsic* small polaron conductivity to the p-type conductivity of LSCN2020 results in a total "predicted" conductivity (plotted as the thick dashed line in Fig. 15) that agrees well the "true" measured electronic conductivity of LSCN2020. Most interesting is the fact that the "S-shaped" trend with respect to temperature seen in the measured conductivity of LSCN2020 is also predicted by a mechanism including both metallic-like p-type charge carrier and small polarons. The S-shaped trend was also found for all other compositions of $(La_{1-x}Sr_x)_sCo_{1-y}Ni_yO_{3-\delta}$ reported previously.

This could possibly indicate that electronic conduction of LSCN2020 can be described by a dual mechanism where the *p*-type charge carrier as a result of Sr-substitution follows a metallic-like conductivity and where the *intrinsic* charge carrier from e.g. spin transitions on Co ions follows a small polaron conduction mechanism.

There are uncertainties associated with such a simple explanation to the conductive behavior of $(La_{1-x}Sr_x)_sCo_{1-y}Ni_yO_{3-\delta}$. The data presented covers only a temperature span of roughly RT to 1000 °C. Moreover, both crystal and electronic band structure is often more complicated in oxides as compared to metals. For instance Mineshige et al. [5] have studied the conductivity of $(La_{1-x}Sr_x)_sCoO_{3-\delta}$ and found a metal–insulator transition at a critical Co–O–Co angle of 165° irrespective of *x*, *T* and P_{O_2}. Figs. 9 and 10 found a slightly higher mobility for LSCN3010 and LSCN4010 at the lowest measured temperature indicating that the p-type mobility might not be independent on temperature over the entire temperature span RT-1000 °C.

4.3. Expansion behavior

The measured *apparent* thermal expansion coefficients (TEC) shown in Fig. 11 for LSCN4010 and LSC40 illustrate that substituting 10% Co with Ni in LSC40 decreases the TEC across the entire temperature range. The difference is remarkable, about 20–25%, making LSCN4010 an interesting composition for technological use in SOFC-cathodes as it could possibly reduce the large expansion mismatch between the highly electrocatalytic $(La_{0.6}Sr_{0.4})CoO_{3-\delta}$ and the other components of an SOFC.

Substitution of Co with Ni in $(La_{1-x}Sr_x)_sCo_{1-y}Ni_yO_{3-\delta}$ decreases the thermodynamic stability of the perovskite which could result in partial decomposition of LSCN4010 into secondary phases of the type K_2NiF_4-type and CoO/NiO when reaching temperature as high as 1300 °C [43,44,15]. We have previously shown support that secondary phases of transition metal oxides in $(La_{1-x}Sr_x)_sCo_{1-y}Ni_yO_{3-\delta}$ are of NiO. The origin of the sharp peaks in the differential expansion curve of LSCN4010 at 630 and 1050 °C will not be fully explained in this paper. However, a possible explanation could be a reaction between the NiO and a K_2NiF_4-type oxide to regain the perovskite structure upon cooling. Such a reaction would involve an uptake of gaseous oxygen expanding the lattice momentarily. The fact that these artifacts were not seen in the repetitive experiment to 1100 °C indicates that this temperature and time (1 h) is not sufficient to adequate amounts of secondary phases.

To describe the thermal expansion behavior of oxides only in terms of a coefficient is somewhat misleading and certainly not sufficient in the case of $(La_{1-x}Sr_x)_sCo_{1-y}Ni_yO_{3-\delta}$. The *apparent* TEC is seen to increase continuously above approximately 500 °C for both LSC40 and LSCN4010, a temperature that correlates well with the onset temperature of oxygen loss seen in Fig. 4. The increase in the *apparent* TEC at higher temperatures has in previous papers been argued to be related to the thermal reduction of Co(IV) to Co(III) which expands the Shannon radius from 0.53 Å for Co^{4+}(VI) (HS) to 0.61 Å for Co^{3+}(VI) (HS) [6]. This expansion is often referred to as the chemical expansion and relates to the oxygen nonstoichiometry change with the chemical expansion coefficient (CEC). However, also the CEC should not be regarded as a simple coefficient, which the following paragraph attempts to justify.

Fig. 4, shows clearly that δ increases linearly with *T* above a certain threshold temperature (expressed in Eq. (8)). In the case of LSC40 and LSCN4010 this temperature is approximately 700 °C. Now if the lattice expansion was found to be dependent on *T* and δ only to a first order then the *apparent* TEC would be expressed as the sum of two constants, TEC_{500} and TEC_{700}, where the later is valid only above approximately 700 °C. This is expressed in Eqs. (9)–(11) where α is the expansion coefficients with respect to temperature, β is the expansion coefficients with respect to δ and γ is the linear coefficient with which δ increases with temperature above 700 °C:

$$\delta = (\gamma \cdot T)_{T \geq 700\,^\circ\mathrm{C}} \tag{8}$$

$$\varepsilon = \alpha \cdot T + \beta \cdot \delta = \alpha \cdot T + \beta \cdot (\gamma \cdot T)_{T > 700\,^\circ\mathrm{C}} \tag{9}$$

$$TEC_{500} = \left(\frac{\partial \varepsilon}{\partial T}\right)_{T \leq 500\,^\circ\mathrm{C}} = \alpha \tag{10}$$

$$TEC_{700} = \left(\frac{\partial \varepsilon}{\partial T}\right)_{T \geq 700\,^\circ\mathrm{C}} = \alpha + \beta \cdot \gamma \tag{11}$$

This would result in an *apparent* TEC having an s-shaped curve with a constant value of α below 500 °C and another constant value of $\alpha + \beta \cdot \gamma$ above 700 °C. However, the *apparent* TEC, shown in Fig. 11, continues to increase in the high temperature region for both LSC40 and LSCN4010. This suggests that the CEC is not a single order coefficient but depends on δ and/or *T* to a second order degree. Additionally, the *apparent* TEC of LSC40 appears to increase below 500 °C where δ is approximately zero.

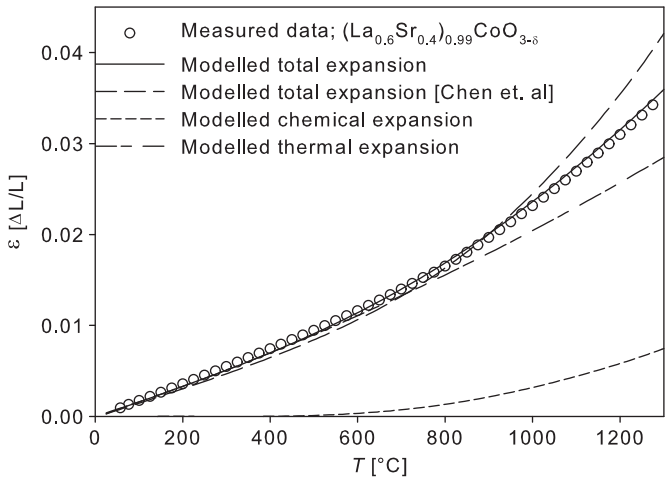

Fig. 16. Expansion as function of temperature for LSC40 reported in Fig. 11 where it is differentiated with respect to temperature. Lines represent the predicted expansion according to 6, where δ was taken from Fig. 4 and the expansion coefficients from Table 3.

This indicates that also the true TEC is dependent on T to a second order degree. This motivated us to characterize the expansion behavior of $(La_{1-x}Sr_x)_sCo_{1-y}Ni_yO_{3-\delta}$ using the mechanism expressed in Eq. (6). This model was first tested by Adler and coworkers in a study on lattice expansion behavior of $(La_{1-x}Sr_x)_sCoO_{3-\delta}$ [21].

As seen in Figs. 12–14 this expansion model was found to fit the measurements on LSC40, LSCN3010 and LSCN4010 well. Comparing LSCN4010 and LSC40 using the results in Table 3 shows that substituting 10% Co with Ni in LSC40 decreases the first order TEC (α_1) substantially. The second order TEC (α_2) is slightly higher for LSCN4010 but calculating the strain up to 850 °C, caused only by heating and not stoichiometric changes ($\varepsilon_{\alpha,850C}$), shows that the strain in LSCN4010 is about 15% lower. This could be explained by the Ni containing composition having less trivalent Co ions which undergoes the electronic spin transition that gives rise to the unusually large *apparent* TEC of these cobaltites. The first order CEC (β_1) of LSC and LSCN4010 was found to be approximately the same, whereas the second order CEC (β_2) is three times larger for LSC40. This is compensated by the higher δ of LSCN4010 as the strains induced exclusively by the chemical expansion when heated to 850 °C ($\varepsilon_{\beta,850\,^\circ C}$) are almost identical.

Comparing α_1 and α_2 of LSCN3010 and LSCN4010 shows that increasing the Sr content will decrease the *true* TEC. The "thermal" strain, ($\varepsilon_{\alpha,850\,^\circ C}$), induced when heated to 850 °C is about 8% lower in LSCN4010. This can again be explained by the lower concentration of trivalent Co ions that can undergo spin transitions upon heating. β_1 appears to increase with Sr substitution whereas β_2 is about four times lower. Calculating the $\varepsilon_{\beta,850\,^\circ C}$-values of LSCN4010 and LSCN3010 shows a 15% lower strain for LSCN3010. This is mainly due to the much lower δ of LSCN3010 within this temperature range.

For LSCN4010 the strain induced by α_2 was found to be about 50% of that induced by α_1 when heated to 850 °C whereas the strain induced by β_2 was about 10% of that induced by β_1. This indicates further that the second order terms are necessary to fully describe the expansion behavior.

The strain in LSC40 as function of temperatures was calculated from the fitting parameters in Table 3 and the oxygen non-stoichiometry shown in Fig. 4 and compared with the strain measured continuously as function of temperature in air (see Fig. 11). The result is reported in Fig. 16 in which we have also include a fit of the strain of $(La_{0.6}Sr_{0.4})CoO_{3-\delta}$ calculated based on expansion coefficients from the study by Chen et al. [21]. The figure shows that the strain calculated from using the coefficients in Table 3 agrees reasonably well with the measured strain. The strain calculated from expansion coefficients of [21] overestimated the expansion above 1000 °C if compared to the measured strain of our sample. Comparing the thermal and chemical expansion coefficients from these two studies shows that the β_2 reported by [21] is more than three times higher than ours which results in a much large expansion increase at high δ (ie high T). It is noteworthy that the major contribution to the strain in LSC40 arises from thermal and not chemical expansion.

5. Conclusions

We have found that the *itinerant electron model* [10], describes the defect chemistry of LSCN2020, LSCN3010 and LSCN4010 well. This indicates that our investigated compositions are of metallic-like character with delocalized electronic states. This is also reflected in the high electronic conductivities measured. The conductivities were shown to be linearly dependent on the p-type charge carrier concentration. The measured conductivities were suggested to consist of an p-type contribution together with an intrinsic contribution arising from electronic spin transitions and Ni substitution. The p-type conductivity was found to have a metallic-like reciprocal temperature dependence above approximately 800 °C. The thermal behavior and conduction mechanism of intrinsic contribution was hypothesized to be of the small polaron type. This contribution to the conductivity was more difficult to describe and further analysis is needed to fully understand the conductivity of these complicated oxides.

Expansion measurements as function of T and P_{O_2} showed that substituting 10% Co with Ni in LSC40 decreased the *apparent* thermal expansion coefficient with 20–25% in the entire measured temperature range (25–1300 °C). The expansion behavior could successfully be described using a model incorporating first and second order thermal and chemical expansion coefficients. Separating the *apparent* TEC showed that Ni substitution into LSC40 appears to decrease both the thermal and chemical expansion coefficients.

References

[1] J. Mizusaki, J. Tabuchi, T. Matsuura, S. Yamauchi, K. Fueki, J. Electrochem. Soc. 136 (1989) 2082.
[2] J. Mizusaki, Y. Mima, S. Yamauchi, K. Fueki, H. Tagawa, J. Solid State Chem. 80 (1989) 102.
[3] J. Mizusaki, Solid State Ionics 52 (1992) 79.
[4] A. Mineshige, M. Inaba, T.S. Yao, Z. Ogumi, K. Kikuchi, M. Kawase, J. Solid State Chem. 121 (1996) 423.
[5] A. Mineshige, M. Kobune, S. Fujii, Z. Ogumi, M. Inaba, T. Yao, K. Kikuchi, J. Solid State Chem. 142 (1999) 374.
[6] M. Sogaard, P.V. Hendriksen, M. Mogensen, F.W. Poulsen, E. Skou, Solid State Ionics 177 (2006) 3285.
[7] P.M. Raccah, J.B. Goodenou, J. Appl. Phys. 39 (1968) 1209.
[8] A.N. Petrov, V.A. Cherepanov, A.Y. Zuev, J. Solid State Electrochem. 10 (2006) 517.
[9] A.N. Petrov, O.F. Kononchuk, A.V. Andreev, V.A. Cherepanov, P. Kofstad, Solid State Ionics 80 (1995) 189.
[10] M.H.R. Lankhorst, H.J.M. Bouwmeester, H. Verweij, J. Solid State Chem. 133 (1997) 555.
[11] A.N. Petrov, V.A. Cherepanov, O.F. Kononchuk, L.Y. Gavrilova, J. Solid State Chem. 87 (1990) 69.
[12] M.S.D. Read, M.S. Islam, G.W. Watson, F. King, F.E. Hancock, J. Mater. Chem. 10 (2000) 2298.
[13] C.N.R. Rao, O. Parkash, P. Ganguly, J. Solid State Chem. 15 (1975) 186.
[14] N. Hamada, J. Phys. Chem. Solids 54 (1993) 1157.
[15] A. Petrov, V. Cherepanov, T. Aksenova, L. Gavrilova, Russian J. Phys. Chem. A Focus on Chem. 80 (2006) S134.

[16] M.H.R. Lankhorst, H.J.M. Bouwmeester, H. Verweij, J. Am. Ceram. Soc. 80 (1997) 2175.
[17] A. Mineshige, J. Izutsu, M. Nakamura, K. Nigaki, M. Kobune, S. Fujii, M. Inaba, Z. Ogumi, T. Yao, Electrochemistry 68 (2000) 515.
[18] C. Zobel, M. Kriener, D. Bruns, J. Baier, M. Gruninger, T. Lorenz, P. Reutler, A. Revcolevschi, Phys. Rev. B 66 (2002) 020402.
[19] S.B. Adler, J. Am. Ceram. Soc. 84 (2001) 2117.
[20] P.V. Hendriksen, J.D. Carter, M. Mogensen, Expansion on reduction, in: S.C. Singhal, M. Dokiya (Eds.), Fourth International Symposium on SOFC, Yokohama, Japan, 1995, p. 934.
[21] X.Y. Chen, J.S. Yu, S.B. Adler, Chem. Mater. 17 (2005) 4537.
[22] P.H. Larsen, P.V. Hendriksen, M. Mogensen, J. Thermal Anal. 49 (1997) 1263.
[23] R.D. Shannon, Acta Crystallogr. Sect. A 32 (1976) 751.
[24] K. Huang, H.Y. Lee, J.B. Goodenough, J. Electrochem. Soc. 145 (1998) 3220.
[25] M. Hrovat, N. Katsarakis, K. Reichmann, S. Bernik, D. Kuscer, J. Holc, Solid State Ionics 83 (1996) 99.
[26] V.V. Kharton, A.V. Kovalevsky, V.N. Tikhonovich, E.N. Naumovich, A.P. Viskup, Solid State Ionics 110 (1998) 53.
[27] P. Hjalmarsson, M. Sogaard, A. Hagen, M. Mogensen, Solid State Ionics 179 (2008) 636.
[28] IUPAC, Commission on Thermodynamics Oxygen International Thermodynamic Tables of the Fluid State 9, Blackwell Scientific Oxford, 1987.
[29] Y. Teraoka, T. Nobunaga, K. Okamoto, N. Miura, N. Yamazoe, Solid State Ionics 48 (1991) 207.
[30] M.A. Senaris rodriguez, J.B. Goodenough, J. Solid State Chem. 118 (1995) 323.
[31] H. Obayashi, T. Kudo, Jpn. J. Appl. Phys. 14 (1975) 330.
[32] C. Kittel, Introduction to Solid State Physics, John Wiley & Sons Inc, 1996.
[33] H.M. Zhang, N. Yamazoe, Y. Teraoka, J. Mater. Sci. Lett. 8 (1989) 995.
[34] C.N.R. Rao, M. Seikh, C. Narayana, Spin-state Transition in $LaCoO_3$ and Related Materials, Wiley-VCH Verlag GmbH & Co, 2004.
[35] M.A. Senaris-Rodriguez, J.B. Goodenough, J. Solid State Chem. 116 (1995) 224.
[36] T. Arunarkavalli, G.U. Kulkarni, C.N.R. Rao, J. Solid State Chem. 107 (1993) 299.
[37] M. Abbate, J.C. Fuggle, A. Fujimori, L.H. Tjeng, C.T. Chen, R. Potze, G.A. Sawatzky, H. Eisaki, S. Uchida, Phys. Rev. B 47 (1993) 16124.
[38] T. Saitoh, T. Mizokawa, A. Fujimori, M. Abbate, Y. Takeda, M. Takano, Phys. Rev. B 55 (1997) 4257.
[39] K. Asai, A. Yoneda, O. Yokokura, J.M. Tranquada, G. Shirane, J. Phys. Soc. Jpn. 67 (1998) 290.
[40] S. Yamaguchi, Y. Okimoto, Y. Tokura, Phys. Rev. B 55 (1997) R8666.
[41] R.H. Potze, G.A. Sawatzky, M. Abbate, Phys. Rev. B 51 (1995) 11501.
[42] P. Ravindran, P.A. Korzhavyi, H. Fjellvag, A. Kjekshus, Phys. Rev. B 60 (1999) 16423.
[43] L.Y. Gavrilova, T.V. Aksenova, L.A. Bannykh, Y.V. Teslenko, V.A. Cherepanov, J. Struct. Chem. 44 (2003) 248.
[44] T.V. Aksenova, A.N. Petrov, V.A. Cherepanov, L.Y. Gavrilova, Russian J. Phys. Chem. 80 (2006) 1215.